Textural fabric influence on P-wave velocity anisotropy: an attempt at scaling

Ludmila Adam [a], Marcus Trimble [a], Auke Barnhoorn [b], Maartje Houben [c], Richard Sykes [d], Lorna J. Strachan[a], Brad Field [d]

[a] *University of Auckland;* [b] *Delft University of Technology;* [c] *Utrecht University;* [d] *GNS Science*
Contact email: l.adam@auckland.ac.nz

Introduction

Elastic wave anisotropy is observed across a range of scales in subsurface rocks (Josh et al. 2012, Hart et al. 2013). The observed anisotropy can result from intrinsic rock mineralogy, mineralogical layering, aligned fractures or anisotropic stress. Elastic wave anisotropy measurements are commonly reported, but separating the contributions of the physical mechanism that cause it is more elusive. Therefore, a better understanding of anisotropy and scale is required to correlate the physical mechanisms that cause anisotropy. Here we attempt to study P-wave anisotropy in the lab at a range of (limited) scales on preserved mudstones extracted from boreholes in the East Coast Basin of New Zealand (Whangai and Waipawa formations). We interpret the elastic wave data by incorporating petrographics, SRA, XRD, CT imaging and SEM analysis. Our study aims to help understand seismic signatures and their relation to the physical properties of organic shales in sonic logs and seismic data.

Methods

We use laser-based ultrasonics to study wave propagation in various settings. A high energy pulsed laser excites ultrasonic waves via thermoelastic expansion of the sample. Ultrasonic waves travel through the sample and are detected using a vibrometer, measuring the displacement at the sample surface due to a wave perturbation (Blum et al., 2013). Figure 1 displays the experimental setup where we show the acquisition geometry for a transmission experiment. We acquire data in rotational (the sample is rotated around the cylinder axis) and linear scan settings. In the latter the waveforms transmit along the sample diameter while the sample is moved laterally. One of the advantages of laser-ultrasound is that elastic waveforms are acquired automatically, densely and quickly. Moreover, the ‘fast’ and ‘slow’ P-wave

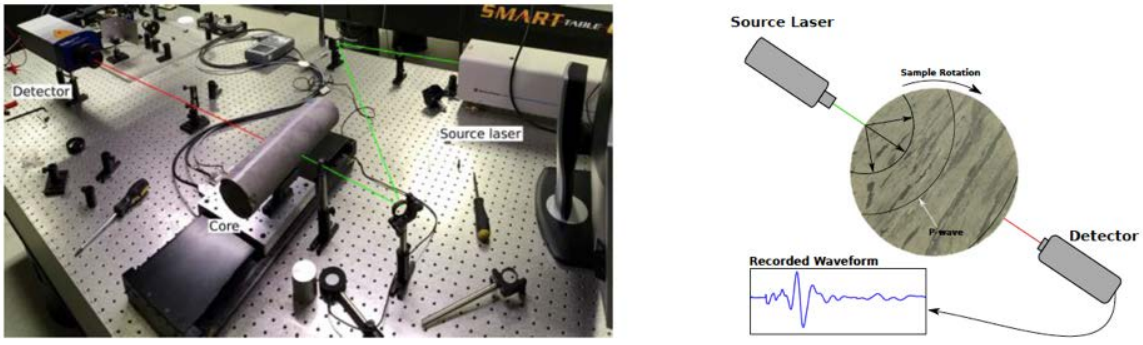

Figure 1. Laser-ultrasonic experimental setup.

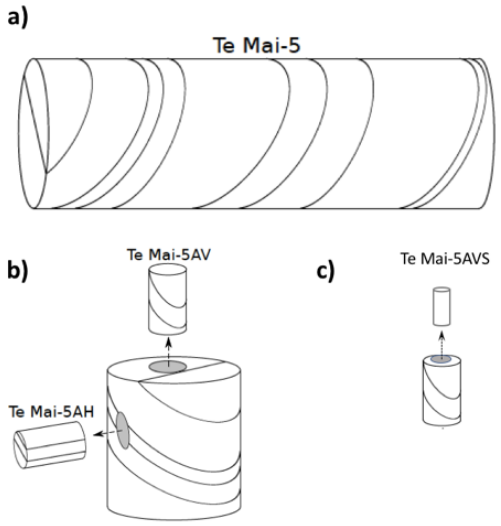

Figure 2. Core sizes and name nomenclature. Core with a diameter of a) 6 cm, b) 2.5cm and c) 0.8 cm.

propagation directions do not need to be known ahead of time and we can validate if the assumption of a vertical transversely isotropic (VTI) media hold for the core sample.

Figure 2 shows a sketch of the preserved core sections and layering direction. Horizontal core plugs (e.g. Te Mai-5AH) are cored parallel to bedding, while vertical cores (e.g. Te Mai-5AV) are cored along the borehole axis. We measured cores with a diameter from 0.8 cm to 6cm and compare their seismic anisotropy to CT images. A total of 5 large (6-8 cm diameter) preserved cores are measured and subsampled. Cylindrical cores are extracted from these and then further subsampled to 0.8 cm diameter.

Results and Discussion

Figure 3 shows the P-wave velocity results of linear and rotational scans on one of the samples. In Figure 3a we show a linear scan acquired in two orthogonal directions (red and blue lines). There is a significant variation in velocities from 3600 m/s to 4200m/s as we scan along the sample. Rotational scans on subsampled cores (red and blue cylinders) are shown in Figure 3c-d. A truly VTI medium would have P-wave velocities with rotational angles closely resembling an ellipse. This behaviour is observed mostly in Te Mai-5AV, but is less evident in Te Mai-5BV. The P-wave anisotropy on the large core (red vs blue line comparison) results in 11.6% and 3.9% for Te Mai-5AV and Te Mai-5BV, respectively. Interestingly, the anisotropy on smaller core samples is in the same range: 13% for Te Mai-5AV and 2.8% for Te Mai-5BV (Figure 3c-d). The observed elastic anisotropy presented in Te Mai-5AV and Te Mai-5BV do not represent the total anisotropy of the core as the layers are tilted with respect to the core vertical axis. However, the visual layering in all samples is consistent (Figure 3b). The full anisotropy is studied on horizontal cores extracted parallel to layering (Figure 2b).

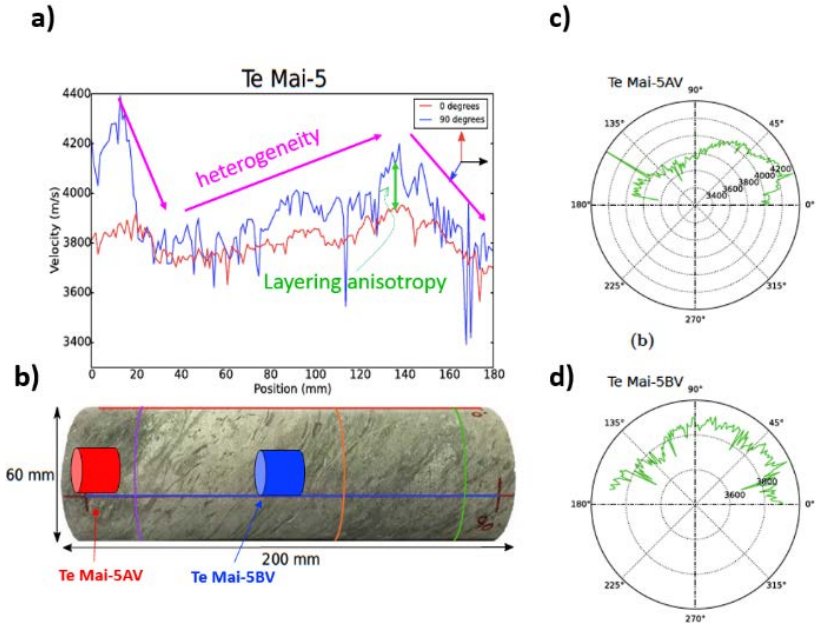

Figure 3. P-wave velocity results from linear (a) and rotational (c and d) scans on samples Te Mai-5. b) is a picture of the core, scan locations and subsampling.

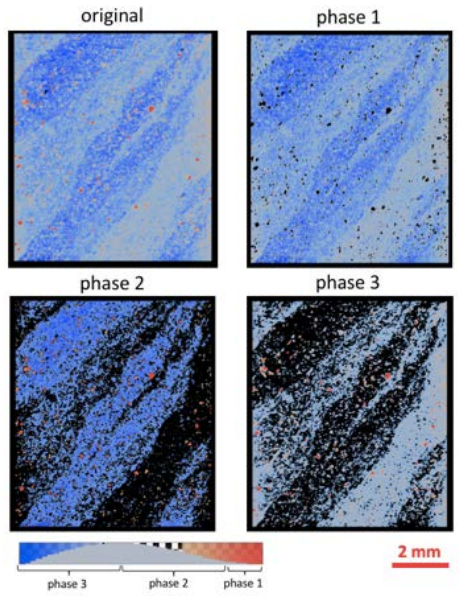

Figure 4. CT scan images for sample Te Mai-5BV. Original refers to the unsegmented image. The definition of the three density phases is based on the histogram shown. Black phase is the segmented area.

Velocity changes along the Te Mai-5 core are of the same magnitude as the elastic wave anisotropy. We will discuss in detail sample heterogeneity and VTI symmetry anisotropy for our samples. Preliminary data shows that heterogeneity in our large cores mostly results from mineralogical different layers. For example, for sample Te Mai-5 the kerogen volume is constant along the core, but there are minor differences in clay content. Visually, some samples show no layering, but high elastic wave anisotropy. In other cases, the obvious pervasive texture does not result in P-wave anisotropy.

To answer some of the questions regarding how texture, mineralogy and composition influence our elastic wave velocities we complemented the laser-ultrasonic data with petrography, XRD, SRA, CT and SEM imaging. Figure 4 shows a CT scan image on sample Te Mai-5BVS. The CT resolution on this sample is 12 µm. The image is segmented in 3 phases based on the histogram. Higher densities are associated with pyrite and carbonate minerals. Variations in density in phase 2 and 3 is inferred from petrographics to depend on porosity and organic content and, to a lesser extent, mineralogy. Quantifying these phase variations will be studied from SEM analysis following similar procedures as in Houben et al. (2016).

The CT scan information is integrated with the elastic data scans. The heterogeneity in phase distributions and the P-wave anisotropy on a range of samples is compared. Preliminary results are shown in Figure 5. It is clear that the phase contribution is variable along the sample. Unfortunately, the velocity scans were acquired prior to CT analysis and happen to be in the location of a similar phase volume. We will present results on the radial distribution of phases from CT imaging as compared to P-wave anisotropy.

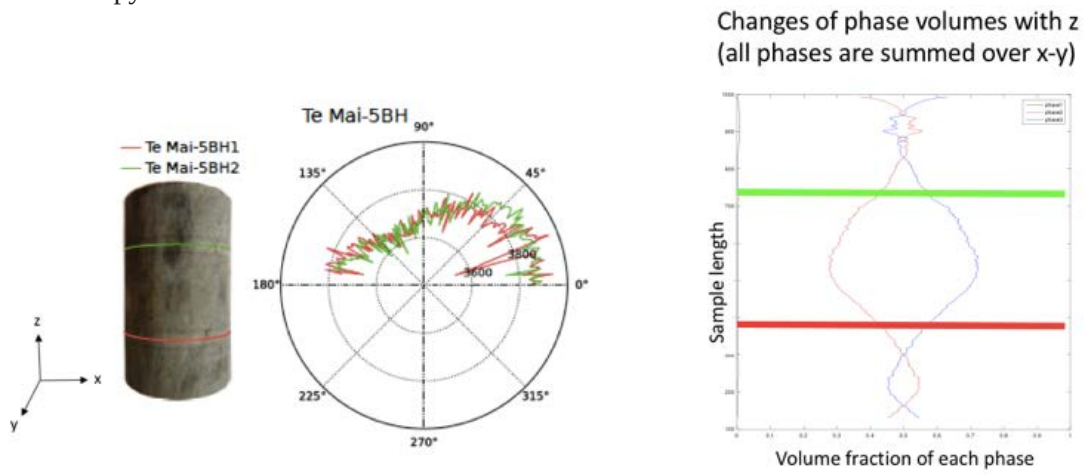

Figure 5. P-wave velocity rotational scan on a horizontal sample at two locations (red and green). The velocity data is compared to the phase volume variations along the z-axis.

Finally, Figure 6 is a plot of transducer ultrasonic velocities as a function of the sum of kerogen volume (estimated from TOC) and clay volume from XRD analysis. For this set of samples spanning the Whangai and the Waipawa formations of the East Coast Basin of New Zealand a general correlation between composition and P-wave velocity is observed. Directionality of wave propagation within a formation shows a variation of up to 500 m/s.

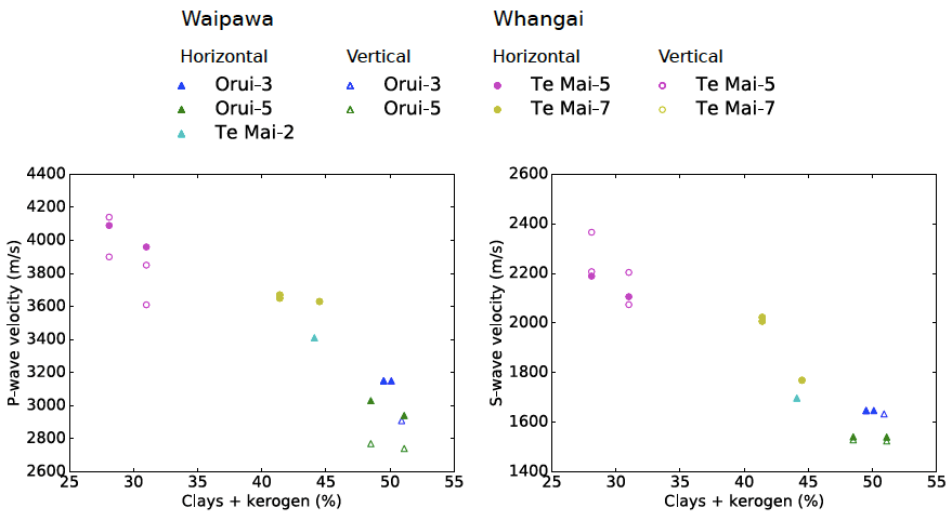

Figure 6. P- and S-wave velocity as a function of clay and kerogen volume for samples from the Waipawa and Whangai formations.

Conclusions

Based on the elastic wave laser ultrasonic data we have made the following primary observations:

- Changes in composition and/or porosity along a sample can cause velocity variations as large as those due to intrinsic anisotropy (up to 15%).
- For sample Te Mai-5 P-wave velocity anisotropy is scale-independent at the cm scale, but varies significantly between adjacent locations.
- Visual sample texture cannot be correlated to wave velocity. Samples with no visual layering (e.g. Te Mai-2 samples) can have significant anisotropy, while in other cases sample with visual layering (e.g. Te Mai-7 samples) have no VTI anisotropy or have heterogeneous wave velocities.
- The presence of fractures modifies the P-wave velocity elipticity, biasing the estimates of P-wave velocity anisotropy.

Compositional effects on wave velocity are studied with TOC, XRD and SEM analysis. Density-based phase distribution is quantified based on CT imaging and compared to elastic wave anisotropy. The contribution of soft phases - kerogen and clays - provides the first order effect on elastic wave velocity. Whangai Formation samples (e.g. Te Mai 5) have a lower clay and kerogen content and thus have higher P- and S-wave velocities. Waipawa Formation samples are higher in both kerogen and clay volumes and have lower wave velocities. The focus of our study is to also understand and quantify velocity variations within each formation which can be up to 500 m/s (20%). We want to better understand the effects on wave velocities that result from layering due to porosity variation, instrinsic clay anisotropy, fractures and kerogen content in the context of heterogeneity vs. VTI anisotropy.

Acknowledgements

We thank the NZEC for providing the core and Bill Leask for fruitful discussions. We thank Wim Verwaal and Ellen Meijvogel-de Koning at TU Delft for their guidance and help with the CT imaging of the samples. This project is partly funded by the Ministry of Business, Innovation and Employment

through the GNS Science-led research programme on New Zealand petroleum source rocks, fluids, and plumbing systems (contract C05X1507).

References

Blum, T. E., Adam, L., & Van Wijk, K. (2013). Noncontacting benchtop measurements of the elastic properties of shales. *Geophysics*, *78*(3), C25-C31.

Hart, B. S., Macquaker, J. H., & Taylor, K. G. (2013). Mudstone ("shale") depositional and diagenetic processes: Implications for seismic analyses of source-rock reservoirs. *Interpretation*, *1*(1), B7-B26.

Houben, M. E., Barnhoorn, A., Lie-A-Fat, J., Ravestein, T., Peach, C. J., & Drury, M. R. (2016). Microstructural characteristics of the Whitby Mudstone Formation (UK). *Marine and Petroleum Geology*, *70*, 185-200.

Josh, M., Esteban, L., Delle Piane, C., Sarout, J., Dewhurst, D. N., & Clennell, M. B. (2012). Laboratory characterisation of shale properties. *Journal of Petroleum Science and Engineering*, *88*, 107-124.